Chemical Physics Letters 760 (2020) 138007

Contents lists available at ScienceDirect

Chemical Physics Letters

journal homepage: www.elsevier.com/locate/cplett

Research paper

Flexible and high-energy dense yarn-shaped supercapacitor based on Ni-carbon nanotubes framework

Didarul Islam [a,*], Md. Helal Uddin [a], Bole Pan [b], Md. M.A. Joy [c]

[a] Department of Applied Chemistry & Chemical Engineering, Islamic University, Kushtia 7003, Bangladesh
[b] Department of Chemistry, Columbia University, New York, NY 10027, United States
[c] Department of Computer Science & Engineering, East West University, Dhaka 1215, Bangladesh

ARTICLE INFO

Keywords:
Oxidized carbon nanotubes
Ni
Sputtering
Yarn supercapacitor
Flexible electronics

ABSTRACT

Herein, we developed a flexible and high-energy dense, solid-state supercapacitor with a yarn-like geometry. In our approach, conductive Ni was sputtered on oxidized carbon nanotubes-coated cotton yarn templates, which were directly used as functional electrodes to construct the supercapacitor. The as-prepared device offered a remarkable specific capacitance of 258.47 mF/cm^2 and a superior energy density of 51.7 μWh/cm^2. The device retained long-term cyclic stability after 5000 cycles of use, with a negligible reduction of electrochemical performance observed under severe bending states. The functional device has great potential to be embedded as a high-performing storage device for versatile miniaturized electronics.

1. Introduction

In recent years, extensive research has been devoted to wearable energy harvesting devices because of the widespread escalation of miniaturized electronic gadgets, smart e-textiles, micro-robotics, wearable computing devices, and implantable medical devices [1,2,20]. Energy harvesting devices are the indispensable parts in powering functional wearable systems; thus, there is a significant scientific and technological importance to develop a safe and lightweight device that could be easily integrated into wearable consumer electronics. Compared with other existing technologies, solid-state yarn supercapacitor (YSC) emerged as a promising candidate as the next generation of portable and wearable storage devices [1–4]. In particular, one-dimensional (1D) yarn-type or fiber-shaped supercapacitors, due to their tiny volume and easy adaptability [1,3,15,16], offer many intriguing features and promising advantages over the conventional bulky sandwich-shaped or planar structure supercapacitors [17,33]. However, a major challenge in this field is the development of a straightforward protocol for fabricating YSC devices without sacrificing the stretchability [19,34] and maintaining the high energy and power density in a single design.

Several novel techniques have been reported in different literature on the fabrication of solid-state YSC device. Kim et al. deposited Ag/MnO_2 composite sheath on carbon nanotube (CNT) yarn substrate, which reached a specific areal capacitance of 322.2 mF/cm^2 and an energy density of 18.3 μWh/cm^2 [5]. Wang et al. fabricated a two-ply YSC using platinum filament reinforced CNT yarn with polyaniline nanowires electrodes and achieved a capacitance of 91.67 mF/cm^2 and an energy density of 12.68 μWh/cm^2 [7]. Kou et al. demonstrated a coaxial wet-spinning assembly strategy to prepare polyelectrolyte-wrapped graphene/CNT core-sheath composite based wet-spun YSCs, achieving a capacitance of 177 mF/cm^2 and an energy density of 3.84 μWh/cm^2 [3]. Undoubtedly, these studies point to a feasible route for the fabrication of YSC. However, their potential application is seriously restricted by the low energy density of the fabricated devices. Therefore, developing a high-energy dense YSC while retaining its intrinsic high-power density is crucial for the supercapacitors real-world electrochemical applications. CNTs have been extensively investigated as electrochemical supercapacitor electrodes because of their highly accessible surface area, excellent electrical conductivity, and high charge transport capability [7,9,10,14,18]. But pure CNT-based YSC possesses a relatively moderate capacitance and low energy density, both of which restrict the practical applications of this device [7]. Surface modification of CNTs through metallization offers a promising approach to improving the electrochemical performance of the YSC [1,7]. For example, Ni modified CNTs configuration can significantly improve the electrical conductivity and the effective charge transportation capability in the YSC device. However, interfacial detachment

* Corresponding author.
E-mail address: didarulislam85@hotmail.com (D. Islam).

https://doi.org/10.1016/j.cplett.2020.138007
Received 6 July 2020; Received in revised form 1 September 2020; Accepted 15 September 2020
Available online 19 September 2020

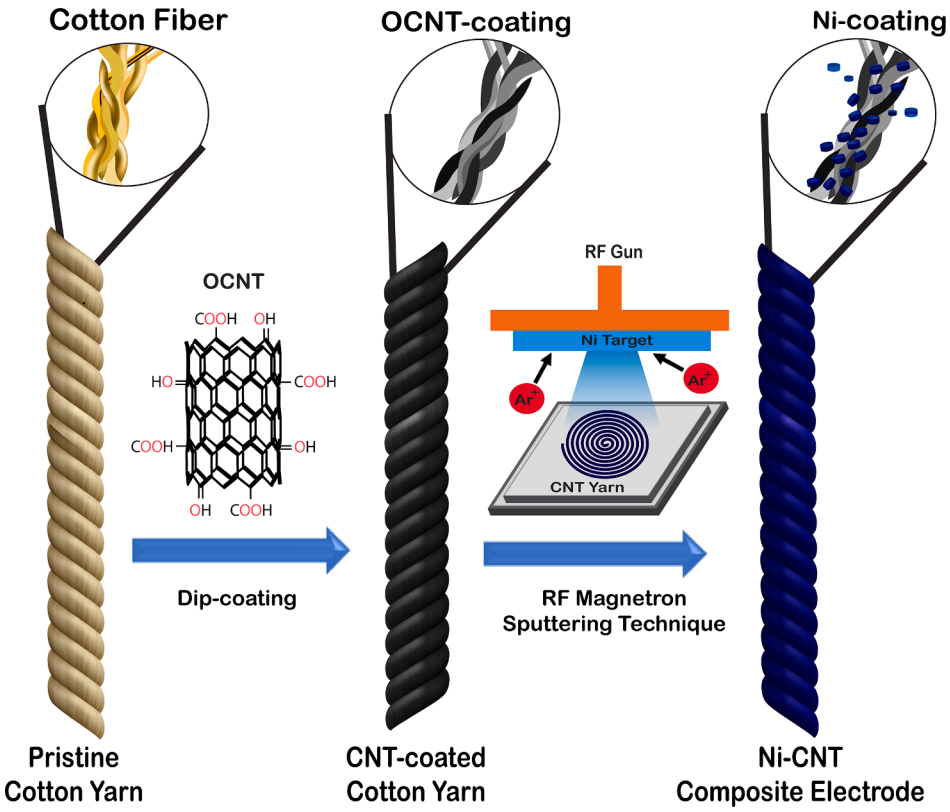

Fig. 1. Schematic illustration of the fabrication of Ni-CNT composite yarn electrode.

between the active electrode material and metallic current collector can drastically reduce the overall electrochemical performance of the supercapacitor [11]. Hence, gaps between CNTs film and the Ni current collector must be engineered to maximize the electrochemical performance.

In this study, we report a convenient method to prepare Ni-decorated CNT composite to further improve the overall electrochemical performance of the CNT-based YSC devices. Hydrophobic multi-walled CNTs (MWCNTs) were converted to hydrophilic oxidized CNTs (OCNTs) by chemical oxidation method to prepare a highly stable monodisperse CNTs ink. Radio frequency (RF) magnetron sputtering technique was applied for directly growing thin metal layer of Ni on one side of the CNT yarn surface. Of many deposition techniques, the RF magnetron sputtering technique was selected in this study because of its advantages including the ease of controlling thickness, film adhesion, uniformity, and the non-requirement of any polymeric or chemical grafting reaction [6]. Our simple surface engineering technique creates a strong synergistic interfacial adhesion between the active electrode material and metallic current collector. The highly stacked Ni layer on CNTs film surface acts as an efficient electron transport pathway and intensely reduce the electrical contact resistance. The experimental results confirmed that the metal deposition has substantially improved the electrochemical performance of the supercapacitor.

2. Experimental section

All chemicals and reagents were purchased from Sigma-Aldrich and used without additional purification except when mentioned specifically.

2.1. Pre-treatment of cotton yarns

The commercial cotton yarns were immersed in ethanol/acetone (5:1 v/v) solution, ultrasonicated for 30 min, and dried at 60 °C for 45 min in vacuum to remove excess oil stains and impurities.

2.2. Preparation of CNT-coated yarns

To chemically oxidize MWCNTs, 10 g of pristine MWCNTs (purity: >95%) were dispersed in 90 ml of H_2SO_4/HNO_3 3:1 (v/v) solution. The whole mixture was heated at 60 °C for 8 h under continuous stirring in a fume hood. Afterwards, the solution was filtered with a 0.1 mm PTFE (poly-(tetrafluoroethylene)) membrane and washed several times with acetone/deionized water (DI) 1:1 (v/v) mixture. Then the solution was filtered with a 0.45 μm pore-sized membrane filter and dried under vacuum at room temperature for 12 h to obtain OCNTs. To prepare ultra-stable and highly monodisperse CNTs ink, the as-synthesized OCNTs were dispersed in 45 ml of DI water with 1 g of sodium deoxycholate (NaDoC, $C_{24}H_{39}NaO_4$) added as surfactant through probe sonication. Subsequently, a pair of pre-cleaned cotton yarn was immersed into CNTs ink solution via dip-coating technique. Finally, the dipped yarns were immersed in ethanol/DI (2:5 v/v) solution and dried in an oven at 80 °C for 3 h to obtain the corresponding CNT-coated cotton yarns.

2.3. Fabrication of Ni-CNT composite yarn electrodes via RF magnetron sputtering technique

Initially, each CNT-coated cotton yarn was rolled like a flat coil sheet (Fig. 1) and wrapped with PTFE tape on one side of the yarn to protect them from sputtering. For deposition, ultra-fine Ni metallic target (~99.999 wt% purity) and RF gun (300 W; 12.56 MHz) were used. The Ni sputtering target was placed 75 mm above the CNT yarn templates. Subsequently, the CNT yarn sample was placed into the substrate holder of a top-down RF magnetron sputtering system (Nano-Master Inc.; NSC-4000). Before the sputtering process, the operating pressure of the chamber was adjusted to a base pressure below 5.33 mbar. The Ni powder was preciously sputtered on one side of the CNT yarn surface at a fixed power of 80 W in an Ar (~99.99%) atmosphere. The deposition

pressure was thoroughly maintained at 6.67 mbar.

2.4. Assembly of YSC

The electrolyte of the YSC device was prepared by mixing 3 g of PVA with 30 ml of DI and then added with 3 g of H_2SO_4. The whole mixture was heated to 90 °C for 2 h under vigorous stirring until a transparent solution was obtained. After this step, a pair of Ni-CNT composite yarn was soaked with the electrolyte solution and allowed to solidify at room temperature for 8 h. Two PVA/H_2SO_4 coated yarns were placed in parallel and twisted together to form the solid-state functional prototype. Finally, they were re-dipped in the electrolyte solution and dried at room temperature for 6 h to improve the adhesion between the electrodes.

2.5. Characterization

The pristine MWCNTs and OCNTs samples were investigated using Fourier-transform infrared (FTIR) spectrometer (PerkinElmer, USA) between 500 and 4000 cm^{-1}. The morphology and elemental analysis of the fabricated yarn was investigated using a field emission scanning electron microscope (FESEM, JSM-7610F, JEOL Ltd.) equipped with an energy-dispersive X-ray spectroscopy (EDX) detector. The X-ray diffraction (XRD) patterns were collected using a diffractometer (Rigaku Ultimate VII) equipped with Cu Kα radiation (λ = 1.540562 Å). The Raman spectra were obtained using a confocal Raman microscope (MonoVista CRS+, S&I GmbH) with a 532 nm wavelength incident laser light.

2.6. Electrochemical measurements

The electrochemical performances were evaluated employing cyclic voltammetry (CV), electrochemical impedance spectroscopy (EIS) and galvanostatic charge-discharge (GCD) measurements using a computerized three-electrode electrochemical work-station (Model CHI 660E by CHI Instrument Inc., USA). The EIS measurements were performed between 0.01 and 100 kHz by applying a sinusoidal voltage of 5 mV. The as-fabricated YSC was directly used as the working electrode, while Pt wire and Ag/AgCl were used as the counter and reference electrodes, respectively. The total surface area (A, cm^2) of the two active electrodes, specific capacitance (Cp, mF/cm^2), energy density (E_D, $\mu Wh/cm^2$), and power density (P_D, $\mu W/cm^2$) of the YSC were computed according to the following equations:

$$A = \pi DL, \tag{1}$$

$$C_P = \frac{I\Delta t}{A\Delta V} \tag{2}$$

$$E_D = \frac{1}{7.2} C_P (\Delta V)^2, \tag{3}$$

$$P_D = 3600 \frac{E_D}{\Delta t}, \tag{4}$$

where, D and L stands for the diameter and length of the yarn electrodes, respectively; I (mA) is the discharge current; Δt (s) is the discharge time; ΔV (V) is the potential window.

3. Results & discussion

Fig. 1 shows the fabrication procedure of Ni-CNT composite yarn electrode. The mass loading of OCNTs of each 1-cm-long composite electrode is 0.1624 mg and the mass of Ni per unit length of the yarn was 0.0375 mg cm^{-1} after sputtering at 80 W for 30 min. The mass loading of OCNTs was controlled by adjusting the dip-coating duration and the mass loading increases with longer dip-coating cycle. The mass loading

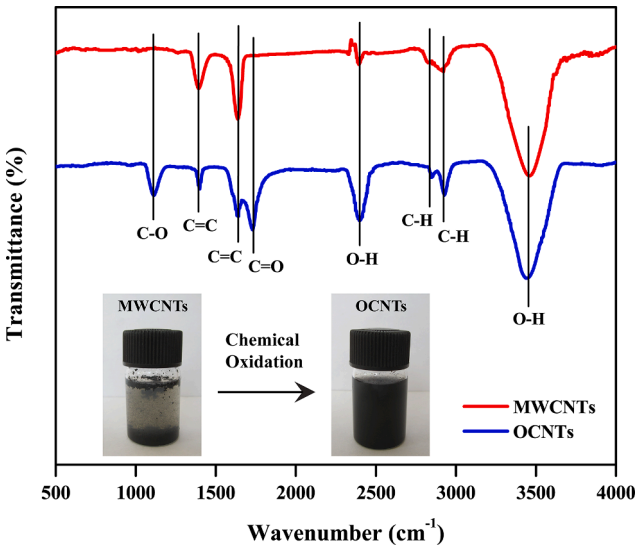

Fig. 2. FTIR spectra of pristine MWCNTs and OCNTs in the range of 500–4000 cm^{-1}.

of OCNTs after dip-coating at 10, 15 and 20 min was 0.1624, 0.1692 and 0.1811 mg cm^{-1}. The mass loading of Ni was 0.0188, 0.0307 and 0.0375 mg cm^{-1} after sputtering at a fixed power of 80 W for 15, 20 and 30 min, respectively, corresponding to 9.43%, 15.35% and 18.79% of the total weight of functional Ni-CNT yarn.

3.1. FTIR analysis

The result of FTIR spectroscopy of pure MWCNTs and OCNTs are shown in Fig. 2. The intense characteristics peak at near 3500 cm^{-1}, which can be identified on both patterns, reflects the stretching modes of the hydroxyl groups [24] and the stretching vibration of the O—H in the carboxyl group [25]. The both MWCNTs and OCNTs samples demonstrate two small peaks at near 2930 cm^{-1} and 2840 cm^{-1}, relating to the C—H stretching vibrations [24,25], which are less intense in MWCNTs sample. The OCNTs revealed two sharp peaks at 2395 cm^{-1} and 1727 cm^{-1}, which can be assigned to the —OH and C═O stretching vibrations of the carboxylic acid (—COOH) groups respectively, [26] which are absent in the pristine MWCNTs. Both samples show aromatic C═C stretching vibrations at near 1635 cm^{-1} and 1400 cm^{-1} [25]. The peak at 1105 cm^{-1} can be attributed to the stretching vibration of C—O bonds, which is located on the ethers in the oxidized CNTs [26]. These characteristic peaks can demonstrate the successful chemical oxidation of MWCNTs that resulted in OCNTs.

3.2. FESEM and EDX analysis

As seen from the FESEM images, smooth, plane and the non-wrinkled surface of pristine cotton yarn fibers (Fig. 3(a)) were modified by the incorporation of OCNTs, resulting in a relatively uneven, cracked and irregular surface for CNT-coated yarn (Fig. 3(b)). The FESEM images of CNT-coated yarn revealed the abundance of OCNTs on the fiber surface. The sputtering phase resulted in the deposition of a thin layer of Ni on the CNT yarn surface. The FESEM images with higher magnification (inset Fig. 3(c)) suggested that metallic Ni penetrated the multiple interval gaps between the individual fibers and densely deposited on the CNT yarn surface. The EDX spectra of Ni-CNT composite yarn are shown in Fig. 3(d). The chemical composition of Ni-CNT composite yarn demonstrates a desirable content of C and Ni with negligible impurities. The presence of oxygen functionalities can be attributed to the chemical oxidization of CNTs. Other elements such as Fe or Al possibly originated from the metal catalyst residue (mainly within the inner of the tubes) of

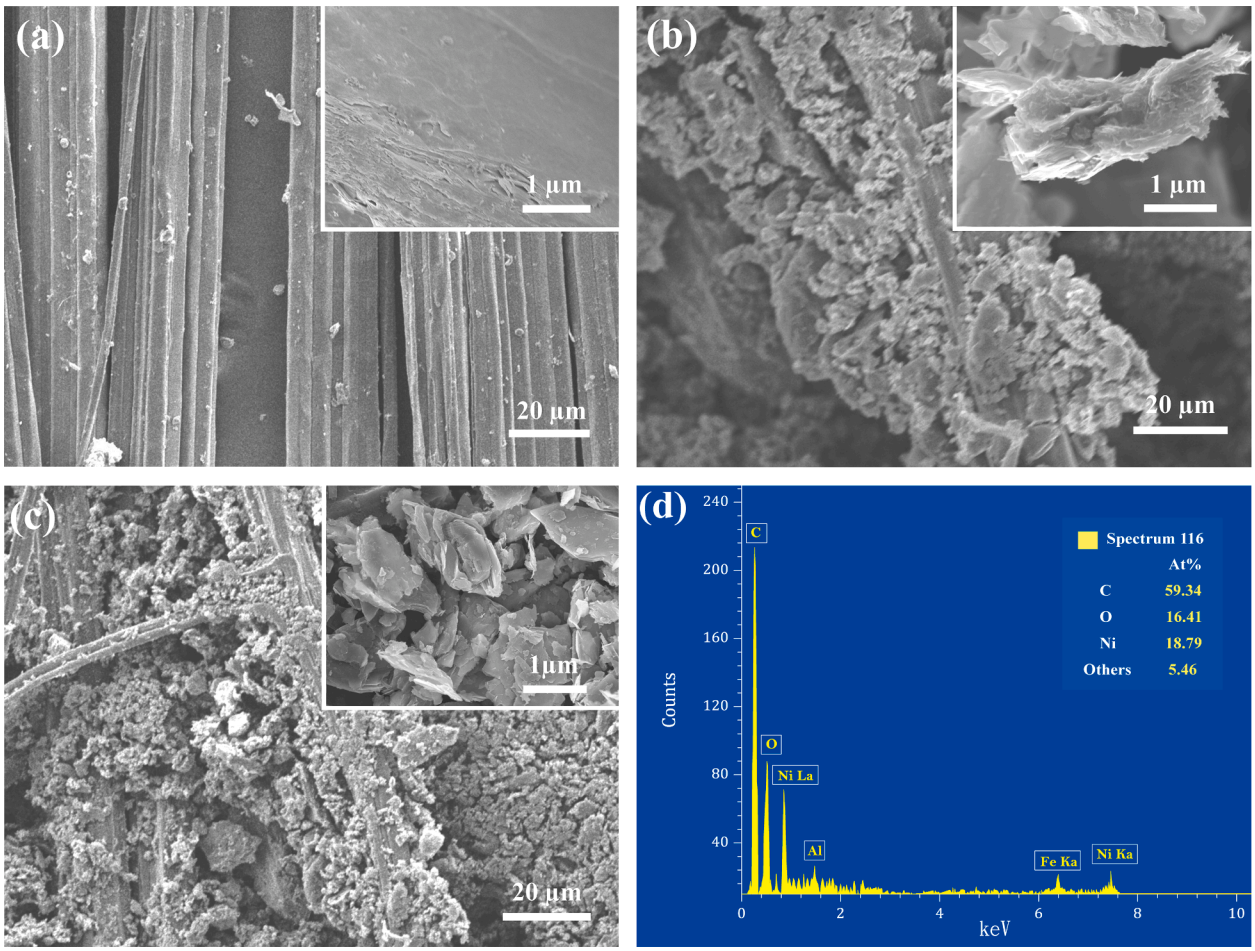

Fig. 3. FESEM micrographs of (a) pristine cotton yarn, (b) CNT yarn, (c) Ni-CNT yarn, & (d) EDX analysis of Ni-CNT yarn.

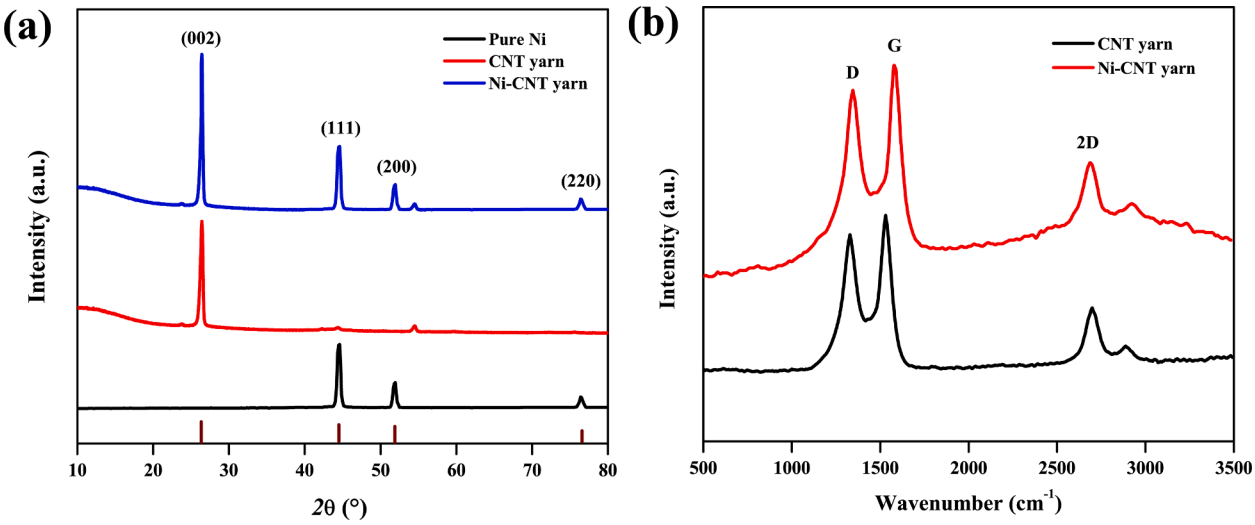

Fig. 4. (a) XRD patterns of pure Ni, CNT yarn, and Ni-CNT yarn, & (b) Raman spectrum of fabricated CNT yarn and Ni-CNT composite yarn.

CNTs. The elemental analysis also confirmed the successful incorporation of Ni onto the CNT yarn surface.

3.3. XRD analysis

The X-ray diffraction patterns of pure Ni, CNT yarn, and Ni-CNT yarn are shown in Fig. 4(a). The distinct peaks at 26.4° in the patterns of CNT yarn and Ni-CNT yarn correspond to the diffraction of the (0 0 2) crystal plane of the CNTs (JCPDS 99-0057). For the pattern of pure Ni, the three peaks at 44.5°, 51.9°, and 76.4° can be assigned to the (111) (200) (220) crystal planes of Ni (JCPDS No. 01–1258). The appearance of the characteristic peaks of both CNT yarn and pure Ni in the pattern of Ni-CNT yarn indicates the successful synthesis of the target electrode with excellent crystallinity.

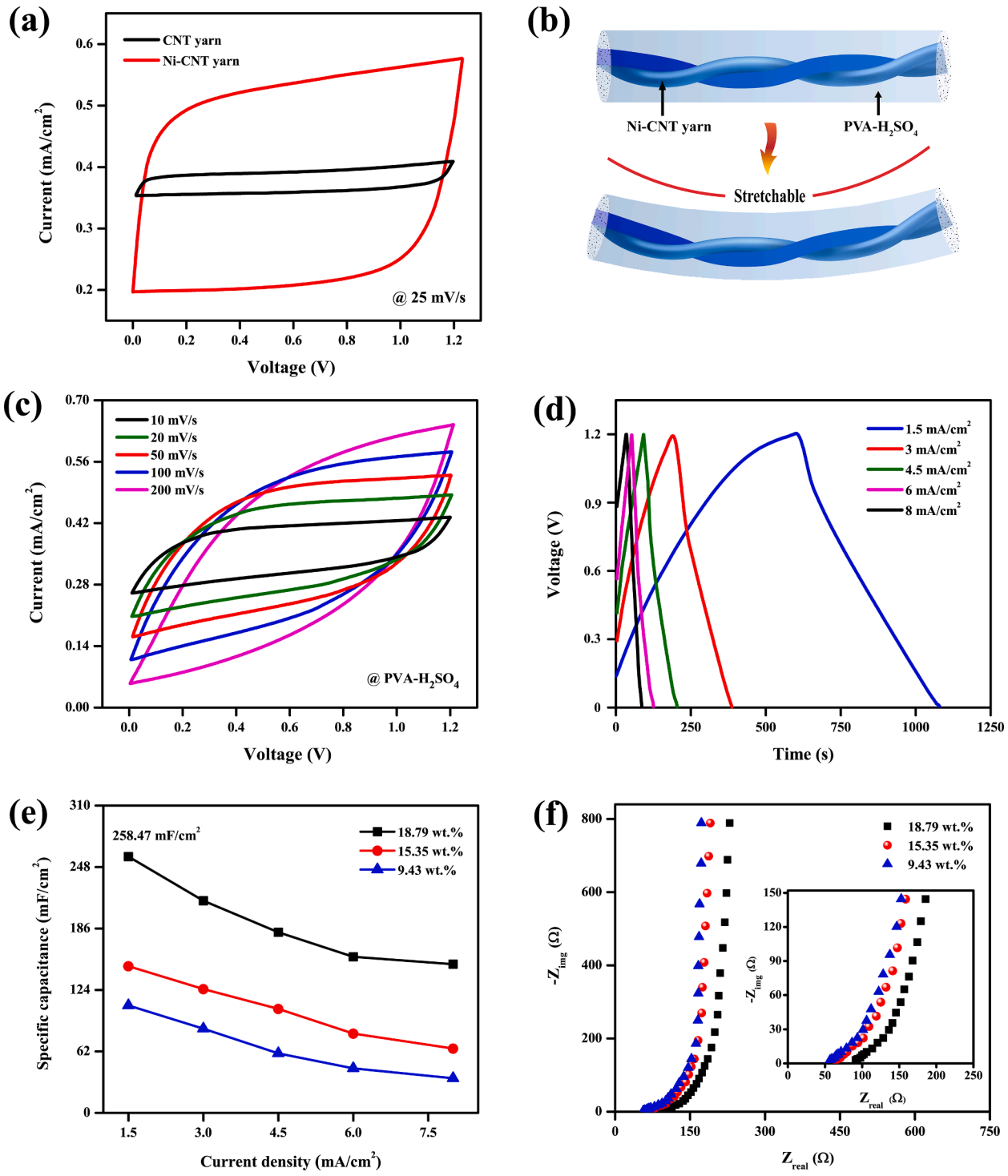

Fig. 5. (a) Comparative CV plots of bare CNT yarn and Ni-CNT yarn containing 18.79 wt% Ni at a scan rate of 25 mV/s in 1 M H_2SO_4 electrolyte, (b) Schematic illustration of the YSC device, (c) CV curves of YSC at different scan rates in PVA-H_2SO_4 electrolyte, (d) GCD curves of YSC at various current densities with a maximum operating voltage of 1.2 V, (e) The relationship between specific capacitance and current density of the YSC with different Ni loadings & (f) Nyquist plot of the YSC with different Ni loadings (The inset shows the high-frequency area).

3.4. Raman spectra analysis

Fig. 4(b) represents the Raman spectrum of fabricated CNT yarn and Ni-CNT composite yarn, which is characterized by three main features including the D, G and 2D mode. The CNT-coated yarn's peak at 1329 cm^{-1}, corresponding to unordered carbon or defects on the CNTs surface [21], is slightly shifted to 1345 cm^{-1} for Ni-CNT composite yarn. The G band is located at 1530 cm^{-1} and 1578 cm^{-1} for CNT-coated yarn and Ni-CNT composite yarn respectively, and this is associated with the C-C stretching in the CNTs lattice [22]. The localized 2D band is at 2698 cm^{-1} and 2689 cm^{-1} for CNT-coated yarn and Ni-CNT composite yarn, respectively, arising from a second harmonic of the D band [23]. The positive shift of the D and G bands and the negative shift of the 2D band after the loading of Ni can be ascribed the acceptor doping of CNT, which, specifically, refers to the minor change in the electronic structure of the CNT resulting from the charge transfer from nanotube walls to the

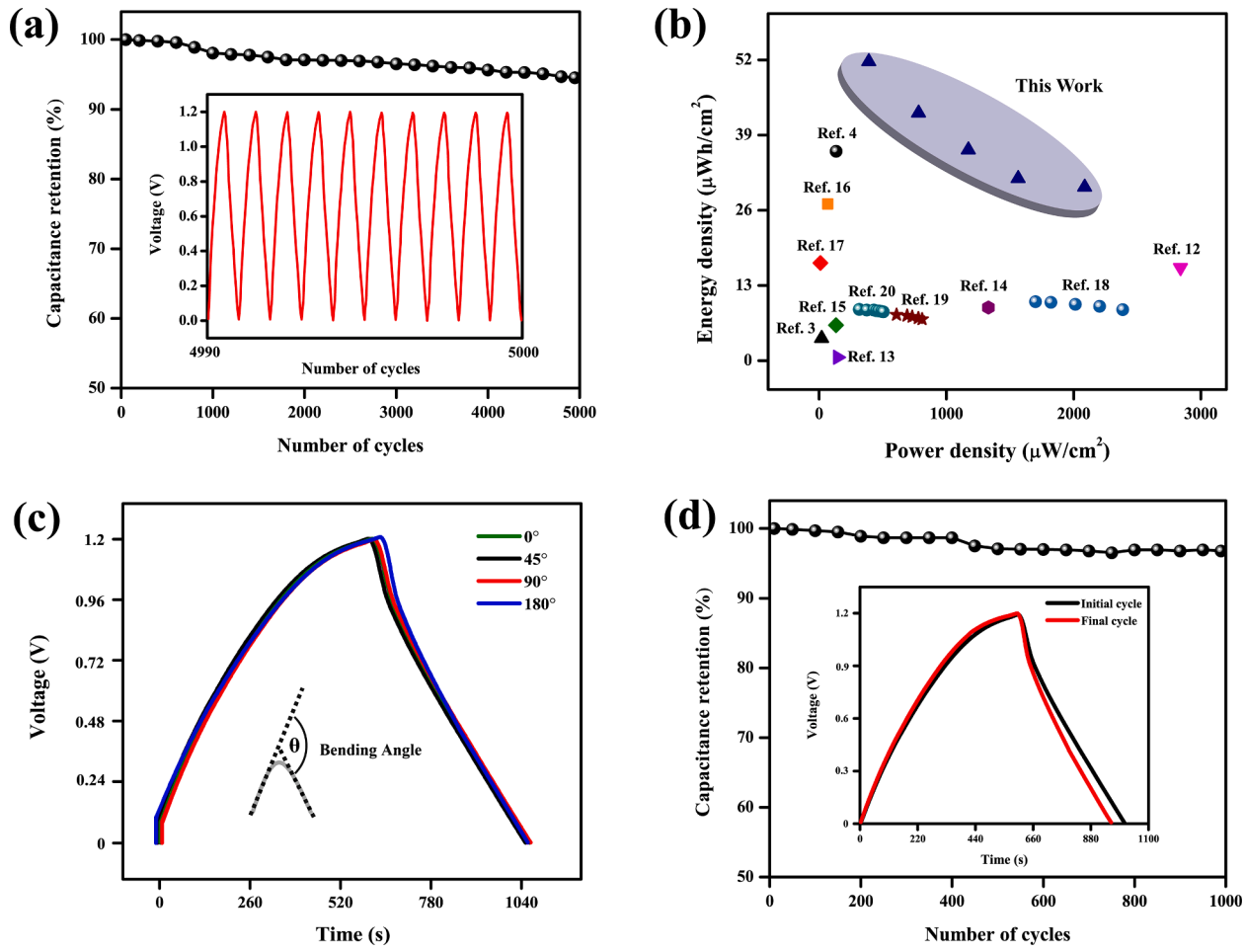

Fig. 6. (a) Cycle life of the YSC prototype (The inset is the GCD curve from the 4990th to 5000th cycle), (b) Ragone plot of the as-prepared YSC device compared to various previously published reports, (c) GCD curves of solid-state YSC at different bending angles & (d) Capacitance retention capability of the YSC under bending at 180° (The inset shows the initial and final GCD curves).

encapsulated salt ions. Small broad peaks are observed at the lower shift values of Ni-CNT composite yarns because of the presence of metallic Ni on the CNTs surface.

3.5. Electrochemical studies

The CV curves for the bare CNT yarn and Ni-CNT composite yarn were measured between 0 V and 1.2 V at a scan rate of 25 mV/s in 1 M H_2SO_4 aqueous electrolyte. As shown in Fig. 5(a), the Ni-CNT composite electrode demonstrates a relatively higher active integral area than CNT yarn electrode. It can be clearly observed that the capacitance contribution of CNT yarn electrode has notably improved after the addition of metallic Ni onto the CNT yarn surface. Based on the superior capacitive characteristics of Ni-CNT yarn, we fabricated the final YSC prototype as shown in Fig. 5 (b) where a pair of composite yarn electrode was assembled together through twisting. Their electrochemical performance was tested using PVA-H_2SO_4 electrolyte. As shown in Fig. 5(c), the CV curves of YSC at different scan rates (10–200 mV/s) exhibit a symmetric and near-ideal rectangular shape. The retention of the shape and structure of the CV curves at higher scan rates indicates an excellent rate capability and the efficient ionic and electronic transports within the electrode materials [8,27,28]. GCD curves for the YSC device were measured at different current densities (Fig. 5(d)) ranging from 1.5 to 8 mA/cm^2 with a maximum operating voltage of 1.2 V. The GCD curves of fabricated YSC exemplify a nearly symmetric triangular shape and rapid responses of current-voltage with no significant ohmic drop. The results from the GCD curves elucidate superior capacitive characteristics and excellent electrochemical reversibility of the YSC device. The calculated maximum specific capacitance (C_P) of YSC device with the highest Ni loading of 18.79 wt% was as high as 258.47 mF/cm^2 at the current density of 1.5 mA/cm^2 and maintained ~58% of initial capacitance at the higher current density of 8 mA/cm^2 (Fig. 5(e)). The results show that the specific capacitance increases with Ni loading. When the Ni loading was decreased almost half-times (from 18.79 wt% to 9.43 wt%), the YSC device still delivers a very high specific capacitance of 108.36 mF/cm^2. The Nyquist plots of the YSC device (Fig. 5(f)) show that the equivalent series resistance (ESR) increases with Ni loading. The estimated ESR of YSC device increased from 56.6 Ω for 9.43 wt% of Ni-loaded electrodes to 91.3 Ω when 18.79 wt% of Ni-loaded electrodes were used. These evidences suggest that the ion diffusion resistance escalates as the yarn becomes thicker when Ni loading increases, and it becomes difficult for the ions to diffuse and access the surface of functional electrodes. Fig. 6 (a) shows the cyclic stability of the YSC device at the current density of 1.5 mA/cm^2. The YSC device demonstrated negligible capacitance degradation and retained 95% of its initial capacitance after 5,000 cycles of use. This excellent life cyclic stability confirms the superiority of fabricated YSC device for practical electrochemical applications. Ragone plot of the as-prepared YSC device compared to various previous reports was illustrated in Fig. 6(b). The maximum energy density was achieved to be as high as 51.7 μWh/cm^2 at a power density of 391.26 μW/cm^2, which is significantly higher than the majority of the recently reported literature. Impressively, the whole device can maintain an energy density of 29.9 μWh/cm^2, even at a high-power density of 2086.9 μW/cm^2. The explanation for the exceptional specific capacitance and high

Table 1
Comparison of the as-prepared YSC with previously published CNT threadlike supercapacitor.

Reference	Electrode materials	Maximum capacitance (mF/cm^2)	Flexibility	Cyclic stability (%)
[29]	CNT@PANI	38	0°-180°	91 (800 cycles)
[10]	CNT@Co_3O_4	52.6	0°-180°	91 (1000 cycles)
[13]	CNT/PEDOT	73	N[b]	92 (10000 cycles)
[30]	SWCNTs/PANI-nanowires	6.23	0°-180°	86 (800 cycles)
[31]	MnO_2/CNTs	3.54	0°-135°	98 (1000 cycles)
[7]	Pt/CNT@PANI	91.67	0°-180°	80 (5000 cycles)
[32]	Au@MnO_2-CNT/ Carbon paper	12	N[b]	90 (2000 cycles)
[12]	SWCNTs/N-doped rGO	116.3	0°-180°	93 (10000 cycles)
This work	Ni sputtered OCNT	258.47	0°-180°	95 (5000 cycles)

N[b] - flexibility tests of threadlike supercapacitors were not given in detail.
SWCNTs - single-walled carbon nanotubes.
rGO - reduced graphene oxide.

energy density lies in the novel structure of the YSC device which can be attributed to three key factors. i) The highly cross-linked and interconnected porous microstructure of Ni-CNT yarn allows fast electron transportation and offers high electrolyte accessibility. ii) The densely grown conductive Ni network on the CNT yarn surface acts as a durable current collector and inherently helps to increases the efficient specific area for ion absorption in the PVA-H_2SO_4 electrolyte. iii) The gap-free interaction between the individual OCNTs with the conductive metallic current collector (Ni) allows rapid charge propagation in the YSC device. The GCD curves for the YSC device under different bending angles (0°-180°) at a current density of 1.5 mA/cm^2 were obtained and shown in Fig. 6(c). The GCD curves maintained a well-linear shape with no significant IR drop and nor observable reduction in their electrochemical performance. The solid PVA-H_2SO_4 electrolyte acts as a separator between the yarn-electrodes and prevents the short-circuit when they are too close to each other. Additionally, it prevents the risk of electrolyte leakage in the functional prototype during occasions of severe bending. The capacitance retention capability of the YSC device under bending at 180° was illustrated in Fig. 6(d). Only 3.5% decay in specific capacitance was observed after 1000 cycles of test. This suggested that the fabricated YSC prototype possess excellent mechanical flexibility with resistance to fatigue, which is tremendously beneficial for developing truly flexible and wearable devices. Table 1. demonstrates a comprehensive comparison of the as-prepared YSC device with previously published CNT threadlike supercapacitor. The intriguing structural features of the fabricated YSC device gives rise to its remarkably high capacitance and long-term cyclic stability without sacrificing its supreme flexible multi-functionalities than most of the previously published literatures.

4. Conclusions

In summary, we demonstrated the potential of utilizing novel Ni-CNTs framework for fabricating solid-state YSC with a maximum operating voltage of 1.2 V. The novel architecture of the functional device offers an outstanding specific capacitance of 258.47 mF/cm^2 and a superior energy density of 51.7 $\mu Wh/cm^2$ at a power density of 391.26 $\mu W/cm^2$. The device also possesses exceptional life-cycle stability, retaining 95% of its initial capacitance after 5000 cycles of use. Additionally, only 3.5% decay in specific capacitance was observed after 1000 cycles of test under bending at 180°, which demonstrates its outstanding fatigue resistance. Therefore, the fabricated prototype opening up possibilities of being embedded and utilized as a flexible, portable and self-sufficient energy storage device for wearable gadgets and intelligent textiles.

CRediT authorship contribution statement

Didarul Islam: Conceptualization, Methodology, Data analysis, Writing - original draft, Writing - review & editing. **Md. Helal Uddin:** Supervision. **Bole Pan:** Data analysis, Writing - original draft, Writing - review & editing. **Md. M. A. Joy:** Writing - original draft.

Declaration of Competing Interest

The authors declare that they have no known competing financial interests or personal relationships that could have appeared to influence the work reported in this paper.

Acknowledgements

The authors would like to thank the Department of Chemistry at University of Dhaka for providing the electrochemical measurement facilities. We thank Md. Shahriar Hasan at the Ahsanullah University of Science and Technology for assisting with the FESEM and Raman spectroscopy.

This research did not receive any specific grant from funding agencies in the public, commercial, or not-for-profit sectors.

References

[1] L. Liu, Y. Yu, C. Yan, K. Li, Z. Zheng, Nat. Commun. (2015), https://doi.org/10.1038/ncomms8260.
[2] M.K. Jha, K. Hata, C. Subramaniam, ACS Appl. Mater. Interfaces (2019), https://doi.org/10.1021/acsami.8b22233.
[3] L. Kou, T. Huang, B. Zheng, Y. Han, X. Zhao, K. Gopalsamy, Nat. Commun. (2014), https://doi.org/10.1038/ncomms4754.
[4] C. Zhang, Z. Chen, W. Rao, L. Fan, Z. Xia, W. Xu, J. Xu, Cellulose (2018), https://doi.org/10.1007/s10570-018-2126-3.
[5] J.H. Kim, C. Choi, J.M. Lee, M.J.d. Andrade, Sci. Rep. (2018), https://doi.org/10.1038/s41598-018-31611-2.
[6] G.S. Kaliaraj, A. Ramadoss, Mater. Sci. Semicond. Process. (2019), https://doi.org/10.1016/j.mssp.2019.104709.
[7] Q. Wang, Y. Wu, T. Li, D. Zhang, M. Miao, A. Zhang, J. Mater. Chem. A (2016), https://doi.org/10.1039/x0xx00000x.
[8] Q. Zhang, J. Sun, Z. Pan, J. Zhang, J. Zhao, X. Wang, C. Zhang, Y. Yao, W. Lu, Q. Li, Y. Zhang, Z. Zhang, NANO Energy (2017), https://doi.org/10.1016/j.nanoen.2017.06.052.
[9] H. Pan, J. Li, Y.P. Feng, Nanoscale Res. Lett. (2010), https://doi.org/10.1007/s11671-009-9508-2.
[10] F. Su, X. Lv, M. Miao, Small (2014), https://doi.org/10.1002/smll.201401862.
[11] M. Wu, Y. Li, B. Yao, J. Chen, C. Li, G. Shi, J. Mater. Chem. A (2016), https://doi.org/10.1039/C6TA06846D.
[12] D. Yu, K. Goh, H. Wang, L. Wei, W. Jiang, Q. Zhang, L. Dai, Nat. Nanotechnol. (2014), https://doi.org/10.1038/NNANO.2014.93.
[13] Q. Meng, K. Wang, W. Guo, J. Fang, Z. Wei, X. She, Small (2014), https://doi.org/10.1002/smll.201303419.
[14] Y. Huang, H. Hu, Y. Huang, M. Zhu, W. Meng, Z. Pei, C. Liu, C. Zhi, ACS Nano (2015), https://doi.org/10.1021/acsnano.5b00860.
[15] J. Sun, Y. Huang, C. Fu, Z. Wang, Y. Huang, M. Zhu, C. Zhi, H. Hu, NANO Energy (2016), https://doi.org/10.1016/j.nanoen.2016.07.008.
[16] G. Qu, J. Cheng, X. Li, D. Yuan, P. Chen, X. Chen, Adv. Mater. (2016), https://doi.org/10.1002/adma.201600689.
[17] Q. Xu, L. Fan, Y. Yuan, C. Wei, Z. Bai, J. Xu, Cellulose (2016), https://doi.org/10.1007/s10570-016-1086-8.
[18] B.D. Boruah, A. Maji, A. Misra, Nanoscale (2017), https://doi.org/10.1039/C7NR01644A.
[19] C. Choi, S.H. Kim, H.J. Sim, J.A. Lee, A.Y. Choi, X. Lepró, G.M. Spinks, R. H. Baughman, S.J. Kim, Sci. Rep. (2015), https://doi.org/10.1038/srep09387.
[20] J. Yoo, S. Byun, C.-W. Lee, C.-Y. Yoo, J. Yu, Chem. Mater. (2018), https://doi.org/10.1021/acs.chemmater.7b03786.
[21] Z. Zhai, S. Wang, Y. Xu, L. Zhang, M. Yan, Z. Liu, J. Solid State Electrochem. (2017), https://doi.org/10.1007/s10008-017-3699-8.
[22] J.-Y. Zhu, X. Yang, Z.-B. Fu, C. Wang, W.-D. Wu, L. Zhang, Mater. Sci. Forum (2016), https://doi.org/10.4028/www.scientific.net/MSF.852.1349.
[23] H. Cheng, A.D. Su, S. Li, S.T. Nguyen, L. Lu, C.Y. Lim, H.M. Duong, Chem. Phys. Lett. (2014), https://doi.org/10.1016/j.cplett.2014.03.071.

[24] N. Li, B. He, S. Xu, J. Yuan, J. Miao, L. Niu, J. Song, Mater. Chem. Phys. (2012), https://doi.org/10.1016/j.matchemphys.2012.01.074.
[25] L. Stobinski, B. Lesiak, L. Kövér, J. Tóth, S. Biniak, G. Trykowski, J. Judek, J. Alloy. Compd. (2010), https://doi.org/10.1016/j.jallcom.2010.04.032.
[26] J. Cheng, P. Zheng, F. Zhao, X. Ma, Int. J. Biol. Macromol. (2013), https://doi.org/10.1016/j.ijbiomac.2013.04.010.
[27] K. Zhang, L.L. Zhang, X.S. Zhao, J. Wu, Chem. Mater. (2010), https://doi.org/10.1021/cm902876u.
[28] S. Biswas, L.T. Drzal, Chem. Mater. (2010), https://doi.org/10.1021/cm101132g.
[29] K. Wang, Q. Meng, Y. Zhang, Z. Wei, M. Miao, Adv. Mater. (2013), https://doi.org/10.1002/adma.201204598.
[30] J.A. Lee, M.K. Shin, S.H. Kim, H.U. Cho, G.M. Spinks, G.G. Wallace, M.D. Lima, X. Lepró, M.E. Kozlov, R.H. Baughman, S.J. Kim, Nat. Commun. (2013), https://doi.org/10.1038/ncomms2970.
[31] J.-H. Jeong, J.W. Park, D.W. Lee, R.H. Baughman, S.J. Kim, Sci. Rep. (2019), https://doi.org/10.1038/s41598-019-47744-x.
[32] H. Xu, X. Hu, Y. Sun, H. Yang, X. Liu, Y. Huang, NANO Res. (2014), https://doi.org/10.1007/s12274-014-0595-8.
[33] F. Mo, G. Liang, Z. Huang, H. Li, D. Wang, C. Zhi, Adv. Mater. (2019), https://doi.org/10.1002/adma.201902151.
[34] Y. Wang, F. Chen, Z. Liu, Z. Tang, Q. Yang, Y. Zhao, C. Zhi, Adv. Mater. (2019), https://doi.org/10.1002/anie.201908985.